Optical detection of magnetic data using magnetooptic indicators with in-plane magnetization

L.E. Helseth, E.I. Il'yashenko, M. Baziljevich and T.H. Johansen
Department of Physics, University of Oslo, P.O. Box 1048 Blindern, N-0316 Oslo, Norway
email: l.e.helseth@fys.uio.no
PACS: 78.20.Ls, 75.50.Gg
Keywords: Magnetooptical effects, Ferrimagnetics

Abstract

We investigate detection of magnetic data using magnetooptical indicators with in-plane magnetization. A simple model for the magnetooptical detection system is presented. We find that the signal to noise ratio changes strongly with the bit size, the polarization noise and the distance between the magnetic carrier and the indicator. In particular, it is found that within our model a signal to noise ratio of 30 is possible for a bit size of 200 nm. We also estimate the resolution of the system, and find that a spot size of $\sim$ 200 nm can be obtained using a suitably designed solid immersion lens. Finally, we discuss detection of several magnetic tracks simultaneously.

I. INTRODUCTION

Magnetic data storage and readout has long been an active field of research due to the ever increasing demands for faster and better access to stored data. The areal density for information storage on magnetic media has increased at an astonishing rate over the last three decades. From 1970 - 1990 the density increased at a rate of 30% per year. In 1992 IBM introduced the magnetoresistive read-head, and the growth rate increased to 60% per year. A very successful development followed in 1998 when IBM announced giant magnetoresistive spin-valves, and thus boosted the growth rate to 100% per year [1]. As the bit density gets higher, it becomes increasingly difficult and costly to design and construct media, read-head, write head, tracking system and error correction electronics.

Many attempts have been directed towards reading out magnetic data by optical systems, since optical readout systems have many interesting features not possessed by magnetic readout heads [2–5]. However, in most optical systems the resolution is limited by the classical diffraction limit $\sim \lambda/2NA$, where λ is the wavelength of light, and NA is the numerical aperture. A possible way to circumvent this problem was introduced by japanese researchers in the 1980's [4,5]. In 1986, Hatakeyama et al. [4] reported that when a thin magnetic film is positioned normally to the recording medium surface, i.e., similar to a single-pole magnetoresistive head, a higher linear resolution may be expected. To demonstrate the principle, they sputtered a Co-Zr thin film on glass, and added a nonmagnetic mirror. By utilizing the longitudinal Kerr effect, they were able to demonstrate a resolution of $\sim 1\ \mu m$, but claimed that the resolution prospects are much better than this. Soon after, Tokumaru and Nomura demonstrated a different system with approximately the same resolution prospects [5]. Their system consisted of a high permeability thin film placed in perpendicular contact with the recording medium, thus guiding the magnetic signal to a stripe-domain Bi-substituted iron garnet film, which responded to the field variations by changing the width of its stripes. In spite of these two very interesting proposals, no further development has taken place on such hybrid optical and magnetical storage systems.

In this paper we analyze a different approach, based on ref. [6], for optical detection of magnetically stored data and other weak magnetic flux sources. The basic system, shown in Fig. 1, is in principle a polarization microscope which detects the magnetization distribution of a magnetooptic indicator [7–10]. Like most other optical systems, our system is also limited by the classical diffraction limit, but it will be shown that by utilizing a suitable solid immersion lens it is possible to obtain a spot size of $\sim$ 200 nm. If the indicator has virtually no domains and is sufficiently sensitive to external fields, it will redistribute its magnetization within less than a nanosecond, and follow the field [11]. Here we present a simple model, which describes the magnetization in the indicator and the magnetooptical detection system. We evaluate the signal to noise ratio as well as the resolution and the focal depth. Finally, we discuss detection of several magnetic tracks simultaneously.

II. READOUT PRINCIPLE

Today there exists different methods for magnetooptical readout; the single ended detection system of Fig. 1 and the differential detection system of Fig. 2. The differential detection system is a key feature to the success of modern magnetooptical storage devices,

mainly due to its low noise and superior signal. The light source is here a polarized semiconductor laser diode operating at constant output power (in practice the laser's drive current is modulated at several hundred MHz to reduce noise from e.g. mode hopping and mode competition). The light beam from the laser is then collimated and passed through a polarizer to ensure that all the light is x-polarized. This light is then focused by the combined action of an objective and a spherical solid immersion lens (SIL). The SIL is placed in very close contact with a magnetooptic indicator. To obtain the best possible contact, the indicator should be deposited directly onto the surface of the SIL. To reflect the light (both x and y-polarized), a mirror is deposited onto the indicator. This mirror should also function as a protection against wear from the magnetic carrier medium. If this is not sufficient, an additional protective layer (e.g. Ti_3N_4 or equivalent) can be applied. The magnetic carrier is moved while staying in close contact with the mirror/protective layer. Usually an airgap is formed between the two, and the sum of the airgap and the total thickness of the mirror/protective layer will be called the flying height of the carrier, since this corresponds to the actual distance to the magnetic sensor.

The indicator will redistribute its magnetization according to the magnetic source. Furthermore, since the indicator is supposed to have large magnetooptic effect, it will turn some of the incident x - polarized light into y - polarized light. In the return path, the partially polarizing beamsplitter (PPB) provides the detection module with a fraction γ of the x-component and the entire y-component. The x-component, although without significant information, is needed for proper extraction of data [2]. A polarizing beam splitter (PB), with its axes at 45° to the x and y-polarization, splits the beam in two components. Together with detectors 1 and 2, the PB comprise a balanced differential detection module. The detectors are low noise photodiodes, and their signals form the input of a differential amplifier.

III. MAGNETOOPTIC RESPONSE

In order to serve as an indicator, the film must in addition to having a small anisotropy field, also have a large magnetooptic effect, as shown in Fig. 3, and we will here only consider the Faraday rotation. Due to this effect, secondary light beams are generated on the way down and also after reflection from the mirror. The combined action of the mirror and the indicator is represented by the effective reflection matrix

$$\mathbf{R} = \begin{bmatrix} r_x & r_{xy} \\ r_{yx} & r_y \end{bmatrix} \quad .$$

If we assume that multiple reflections and absorption can be neglected, and that the light is normally incident on the indicator, one has $r_x = r_y = 1$ and [13]

$$r_{yx} = -r_{xy} = \frac{2V}{M_s} \int_0^t M_z dz \quad . \tag{1}$$

Here V is a constant characteristic of the indicator, t the thickness and M_s is the saturation magnetization. The z-component of the magnetization is expressed as [14]

$$M_z = M_s \frac{H_z}{H_a}, \quad H_a = M_s - \frac{2K_u}{\mu_0 M_s} \ , \tag{2}$$

where H_a is the anisotropy field and K_u is the uniaxial anisotropy constant. For a Kerr film similar expressions for the reflection coefficients exists [13].

For data stored on tapes and hard discs the magnetic field can be found rather accurately by applying the Landau-Lifshitz-Gilbert equations [1,3]. Such detailed calculations require extensive computational efforts, and will not be considered here. Instead we will follow Hatakeyama et al. [4], who assumed that the field from a source of size b has a z-component given by

$$H_z = M \exp\left(-\pi \frac{z+d}{b}\right) \ . \tag{3}$$

The remanent magnetization of the recording medium, M, will in general depend on the bit size and the configuration of the neighbour bits. However, we will take it to be constant with $M = 100$ kA/m. We also neglect the presence of an in-plane magnetic field, since the main effect of such a component is to increase the effective anisotropy field, and thereby reducing the sensitivity. The eq. (1) and eq. (3) give then the following magnetooptic coefficient

$$r_{yx} = \frac{2VMb}{\pi H_a} \exp\left(-\frac{\pi d}{b}\right) \left[1 - \exp\left(-\frac{\pi}{b}t\right)\right] \ . \tag{4}$$

We define the polar Faraday rotation as

$$\Theta = \frac{r_{yx}}{r_x} \ . \tag{5}$$

There are many materials which may function as indicators. In particular, bismuth-substituted ferrite garnet films with in-plane magnetization have been shown to have very little domain activity as well as excellent sensitivity to external fields [7,8,10,15,16]. Fig. 4 shows experimental values for the Faraday rotation (at $\lambda = 633$ nm) as a function of a uniform magnetic field (H_z) for two different garnet films. From the figure we find that $V \sim 1\ \mu m^{-1}$ and $H_a \approx 60\ kA/m$. By shifting the wavelength towards $\lambda = 510$ nm and increasing the bismuth content it is possible to increase V by a factor 10, although at the cost of increased absorption [16].

Shown in Fig. 5 is the Faraday rotation obtained from eq. (4) and eq. (5) as a function of bit size b for two film thicknesses and d=100 nm. One sees that for detection of bits smaller than 0.5 μm one gains very little by using garnets thicker than 0.5 μm. Fig. 6 shows the calculated Faraday rotation as function of bit size for different flying heights d when $t = 0.5\ \mu m$. Note that the signal is strongly dependent on the flying height. We find that flying heights of less than 100 nm are required to obtain 0.1 degree rotation when b = 200 nm.

IV. SIGNAL TO NOISE RATIO

To calculate the signal to noise ratio, we will use the model considered in the previous section. Let us assume that the incident beam consists of x - polarized light only, and has

intensity $I_0 = |E_0|^2$. The light is first transmitted through the isotropic GGG substrate, and then reach the magnetooptic layer, where some fraction is transformed into y-polarized light. After reflection the rays are transmitted once more through the substrate before they reach the analyzer. Then the normalized electric field components just before the analyzer can be written as $E_x = r_x = 1$ and $E_y = r_{yx}$. Here we have neglected all differences in transmission coefficients for x and y-polarized light.

For various reasons, there are fluctuations in the effective reflectivity of the s and p-component of the polarization. First, the creation of domains and the redistribution of magnetization will vary rapidly with the magnetic signal, and this may give rise to a y-polarized noise component. Second, the noise from the magnetic carrier may have its own noise which is transferred to the optical signal in the form of y-polarized noise. Third, there are residual amounts of vibration and defocus errors that vary with time and, therefore, cause the x-polarized reflectivity to fluctuate. However, this class of noise is rather common to most readout devices (depend on mechanical design), and will not be considered here. We will follow the procedure given by Mansuripur in dealing with the noisy signal [2]. In this approach, we write the x and y-component of the reflectivity as

$$r_x(t) = 1 + \delta_x(t) \ , \ \ |\delta_x| \ll 1 \ \ , \tag{6}$$

and

$$r_y(t) = 1 + \delta_y(t) \ , \ \ |\delta_y| \ll 1 \ \ . \tag{7}$$

There is also a conversion from x to y-polarized light not caused by the magnetooptic effect, but rather by random scattering events. This can be expressed as

$$r_{xy}(t) = \delta_{xy}(t) \ , \ \ |\delta_{xy}| \ll 1 \ \ , \tag{8}$$

We do not expect this component to be large, since the optical system is at rest, thus reducing all random scattering events to a minimum. We will ignore all correlations between δ_x, δ_y and δ_{xy}, and treat these parameters as independent random variables. Finally, we must take into account the laser noise δ_l, which is rooted in instabilities in the laser cavity (e.g. mode hopping and mode competition). The laser noise is common to both x and y-polarized light. The root mean square values of the fluctuation parameters are defined as

$$\Delta_\alpha = \sqrt{< \delta_\alpha^2 >} \, , \ \ \alpha \, = \, x, \, xy, \, y, \, l \ \ . \tag{9}$$

For the rest of the paper we will assume that all the signals and fluctuations are real-valued. The intensity reaching the individual detectors in Fig. 2 can be given as

$$I_{1,2} = |\frac{E_0}{\sqrt{2}}(1 + \delta_l) \left[\gamma E_x(1 + \delta_x) \pm E_y(1 + \delta_y) \pm E_x\delta_{xy}\right] |^2 \ \ , \tag{10}$$

where + and − corresponds to detector 1 and 2, respectively. To first order this expression becomes

$$I_1 = \frac{1}{2} I_0 \left[(\gamma E_x + E_y)^2 + (\gamma E_x + E_y)[E_x\gamma(\delta_l + \delta_x) + E_x\delta_{xy} + E_y(\delta_l + \delta_y)]\right] \ \ , \tag{11}$$

$$I_2 = \frac{1}{2} I_0 \left[(\gamma E_x - E_y)^2 + (\gamma E_x - E_y)[E_x \gamma(\delta_l + \delta_x) - E_x \delta_{xy} - E_y(\delta_l + \delta_y)] \right] \ . \tag{12}$$

The difference signal between the two detectors is therefore given by

$$I_1 - I_2 = i_{sig} \left[1 + \left(2\delta_l + \delta_x + \delta_y + \frac{E_x}{E_y} \delta_{xy} \right) \right] \ , \tag{13}$$

where the useful signal is

$$i_{sig} = 2\gamma I_0 E_x E_y \ . \tag{14}$$

The noise due to variations in the reflectivities becomes

$$i_{rms}^2 = (i_{sig})^2 \left(4\Delta_l^2 + \Delta_x^2 + \Delta_y^2 + (\frac{E_x}{E_y})^2 \Delta_{xy}^2 \right) \ . \tag{15}$$

Two other inavoidable noise sources are the shot noise and the thermal noise. The shot noise is expressed by

$$i_{shot}^2 = 2e \left| \frac{E_0}{\sqrt{2}} \right|^2 (\gamma^2 E_x^2 + E_y^2) B = e I_0 (\gamma^2 E_x^2 + E_y^2) B \ , \tag{16}$$

where B is the bandwidth of electronic system. The thermal noise is

$$i_{th}^2 = \frac{4kTB}{R} \ , \tag{17}$$

where k is the Boltzmann constant, T is the temperature and R is the load resistance of the differential amplifier.

In total the noise from the differential system is given by

$$i_n^2 = i_{rms}^2 + 2i_{shot}^2 + 2i_{th}^2 \ . \tag{18}$$

Since there are two detectors in the system, the thermal and the shot noise from each of them add together.

The signal to noise ratio (SNR), is defined as

$$SNR = \frac{i_{sig}}{i_n} \tag{19}$$

It should be pointed out that the SNR considered here does not take into account diffraction or interbit crosstalk, and should therefore be regarded as an upper estimate.

To illustrate the behaviour of the SNR in the current model, Fig. 7 shows the SNR as a function of bit size for 3 different flying heights. The parameters used here are $I_0 = 1$ mW, $B = 10$ MHz, $R = 100$ $k\Omega$, $t = 1$ μm, $\gamma = 0.5$, $\Delta_x = \Delta_y = 0$ and $\Delta_l = \Delta_{xy} = 10^{-5}$ in addition to indicator parameters adopted earlier. The figure suggests that it is necessary to keep the flying height less than 100 nm in order to obtain a SNR of 30 for bit sizes around 200 nm. For bit sizes of 1 μm, the SNR can be as large as 500.

Fig. 8 shows the SNR as a function of bit size for different y-polarized noise components Δ_y when $t = 1$ μm and d=100 nm. The main effect of Δ_y seems to be a reduction of the SNR for larger bit sizes, which is due to the fact that the noise increases with increasing magnetooptic signal.

Fig. 9 shows the SNR as a function of flying height for changing Δ_y when $t = 1$ μm, $b = 0.5$ μm. The curves indicate that Δ_y is very important for small flying heights, and should be kept less than 10^{-2} to avoid significant reduction of the SNR.

V. RESOLUTION

A critical parameter is the optical resolution of the system. In order to estimate the resolution, we adopt the method of Ichimura et al. [17]. Since the off-axis reflection coefficients are very small, we neglect their influence on the focusing properties of the system. We also set the refractive index of the SIL to n=2, since this is close to the refractive index of GGG, and the semiconverging (focusing) angle to $\alpha = 60$ degrees. This gives NA=1.73, which is within reach of the current technology. We see from Fig. 10 that it is possible to obtain full-width-half-maximum resolution of ~ 200 nm, although the width is slightly different in the x and y-directions. It is important to note that our system is, unlike most other SIL-systems, not based on evanescent waves, and does not suffer from the stabillity problems possessed by such systems. Finally it is also useful to note that the resolution (and focal depth) may be improved by introducing an appropriate phase-apodizer [18].

VI. EXTENSION TO SEVERAL CHANNELS

The system discussed above was primarily designed for detection of only one channel/track. To extend this to N channels, i.e. to detect of N magnetic data tracks simultaneously, it is necessary to have an optical readout system with larger field of view. One method is here to include the indicator films in a commerically available magnetooptical disk drive. A typical lens used in current optical disk drives is a molded glass aspheric singlet, designed for operation at single wavelength. It is typically 5 mm in diameter, weighs less than 0.1 g, and has a focal length of approximately 4 mm [19]. Its NA is 0.5-0.6, and the field of view covers a circle with diameter around 100 μm. To obtain a thin elliptical illumination beam on the indicator, a cylindrical lens must be inserted in front of the laser. Maeda and Koyonagi found that for an ordinary optical disk drive this has negligible influence on the resolution if the NA is around 0.5 [20]. Then, if the magnetic tracks each has a width of 5 μm, it should be possible to read out 20 tracks simultaneously, each with a bit size down to 0.5 μm.

Another method for increasing the field of view is to use a cylindrical SIL in combination with an imaging lens [6]. A cylindrical SIL will give approximately the same resolution as the spherical SIL. Then, by using a suitable cylindrical or biconic lens to image the tracks onto the pixels, a large field of view and a high optical resolution can exist simultaneosuly.

VII. CONCLUSION

The detection of bits in magnetic media using magnetooptical indicators with in-plane magnetization has been investigated. A simple model for the magnetooptical detection system was presented. Using this model we have calculated the Faraday rotation and signal to noise ratio, assuming that the signal comes from one bit only, and that the system has negligible absorption. The signal to noise ratio was found to vary strongly with the bit size, the polarization noise as well as the distance between the magnetic carrier and the indicator. In particular, our model predicts that a signal to noise ratio of more than 30 is possible for bit sizes of 200 nm at flying heights of less than 100 nm. We also estimate the resolution

and the focal depth of the system. It is shown that an optical resolution of ~ 200 nm is possible using a solid immersion lens.

ACKNOWLEDGMENTS

The authors acknowledge helpful discussions with A. Kozlov. This work was financially supported by the Norwegian Research Council and Tandberg Data ASA.

REFERENCES

[1] K. O'Grady and H. Laidler *J. Magn. Magn. Mater.* **200**, 616 (1999).

[2] M. Mansuripur *The physical principles of magnetooptical recording* first ed. (Cambridge University Press, United Kingdom, 1995)

[3] R. Gambino (editor) and T. Suzuki (editor) *Magneto-optical recording materials* first ed. (IEEE-press, USA, 2000)

[4] I. Hatakeyama, S. Hirono, K. Nonaka and O. Ishii *Appl. Opt.* **25**, 147 (1986).

[5] H. Tokumaru and T. Nomura *IEEE Trans. Mag.* **23**, 2898 (1987).

[6] E.I. Il'yashenko and Tandberg Data ASA, U.S. Patent No. 5.920.538 (1998).

[7] A.V. Antonov, M.U. Gusev, E.I. Il'yashenko and L.S. Lomov *Int. Symp. on Magnetooptics (ISMO'91), USSR, Kharkov* p.70 (1991).

[8] L.A. Jevenko, E.I. Il'yashenko, V.P. Klin, B.P. Nam and A.G. Solovyev *Int. Symp. on Magnetooptics (ISMO'91), USSR, Kharkov* p.147 (1991).

[9] A.I. Belyaeva, A.L. Foshchan and V.P. Yur'ev *Sov. Tech. Phys. Lett.* **17**, 762 (1991).

[10] T.H. Johansen, M. Baziljevich, H. Bratsberg, Y. Galperin, P.E. Lindelof, Y. Shen and P. Vase, *Phys. Rev. B,* **54**, 16264 (1996).

[11] A.Y. Elezzabi and M.R. Freeman *Appl. Phys. Lett.,* **68**, 3546 (1996).

[12] A. Hubert and R. Schafer *Magnetic Domains* 1st ed.(Springer Verlag, Germany, 1998).

[13] A. Hubert and G. Traeger *J. Magn. Magn. Mater.* **124**, 185 (1993).

[14] M. Shamonin, M. Klank, O. Hagedorn and H. Dotsch *Appl. Opt.,* **40**, 3182 (2001).

[15] A. Zvezdin and V. Kotov *Modern magnetooptics and magnetooptical materials*, (IOP Publishing, Bristol, 1997)

[16] L.E. Helseth, R.W. Hansen, E.I. Il'yashenko, M. Baziljevich and T.H. Johansen *Phys. Rev. B,* **64**, 174406 (2001).

[17] I. Ichimura, S. Hayashi and G.S. Kino *Appl. Opt.* **36**, 4339 (1997).

[18] L.E. Helseth *Opt. Commun.* **191**, 161 (2001).

[19] J.M. Sasian and M. Mansuripur *Appl. Opt.* **38**, 1163 (1999).

[20] T. Maeda and H. Koyanagi *Appl. Opt.* **37**, 8167 (1998).

FIGURES

FIG. 1. Setup for magnetooptic imaging using an indicator film with in-plane magnetization.

FIG. 2. Basic differential detection setup for magnetooptic detection using an indicator film with in-plane magnetization.

FIG. 3. The magnetooptic conversion process. The dashed lines represent the secondary light generated by the magnetooptic conversion. To clarify the generation of the secondary light, we have given the incoming light a small angle from the normal, although the analysis in the text assumes normal incident. Note that secondary light is generated both on the way down and also on the way back into the optical system. Thus, the Faraday rotation is ideally doubled.

FIG. 4. Faraday rotation at wavelength $\lambda = 633$ nm as a function of magnetic field for two different garnet films of composition 1) $Lu_{2.2}Bi_{0.8}Fe_{3.8}Ga_{1.2}O_{12}$ and 2) $Lu_{1.7}Y_{0.7}Bi_{0.6}Fe_{3.8}Ga_{1.2}O_{12}$.

FIG. 5. Calculated Faraday rotation as a function of bit size for $\lambda = 633\ nm$ when $t = 0.5\ \mu m$ (solid line) and $t = 5\ \mu m$ (dash-dotted line). The curves were obtained from eq. (4) and eq. (5) with $V = 1\ \mu m^{-1}$, $H_a = 60\ kA/m$ and $M = 100\ kA/m$.

FIG. 6. Calculated Faraday rotation as a function of bit size when $d = 50$ nm (solid line), $d = 200$ nm (dashed line) and $d = 500$ nm (dash-dotted line). The curves were obtained from eq. (4) and eq. (5) with $V = 1\ \mu m^{-1}$, $H_a = 60\ kA/m$ and $M = 100\ kA/m$.

FIG. 7. SNR as a function of bit size when $d = 500$ nm (solid line), $d = 200$ nm (dashed line) and $d = 50$ nm (dash-dotted line). The curves were obtained from eq. (19) with $V = 1\ \mu m^{-1}$, $H_a = 60\ kA/m$ and $M = 100\ kA/m$.

FIG. 8. SNR as a function of bit size when $\Delta_y = 0$ (solid line), $\Delta_y = 0.001$ (dashed line) and $\Delta_y = 0.01$ (dash-dotted line). The curves were obtained from eq. (19) with $V = 1\ \mu m^{-1}$, $H_a = 60\ kA/m$ and $M = 100\ kA/m$.

FIG. 9. SNR as a function of flying height when $\Delta_y = 0$ (solid line) and $\Delta_y = 0.01$ (dashed line). The curves were obtained from eq. (19) with $V = 1\ \mu m^{-1}$, $H_a = 60\ kA/m$ and $M = 100\ kA/m$.

FIG. 10. The normalized time-averaged electric energy density. The solid line shows the profile of the energy density in the y-direction, whereas the dashed line corresponds to the x-direction.

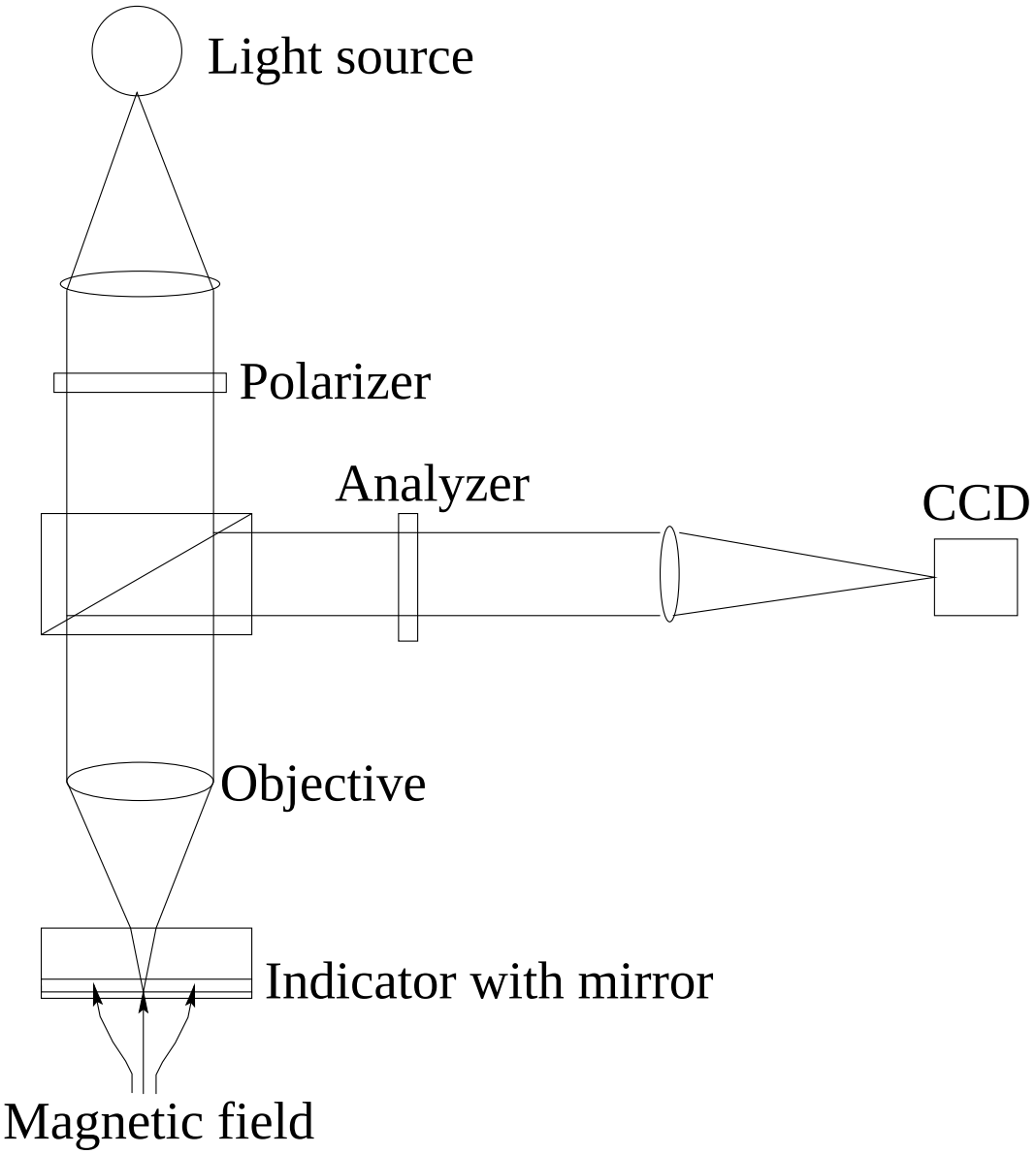
Light source
Polarizer
Analyzer
CCD
Objective
Indicator with mirror
Magnetic field

Figure 1

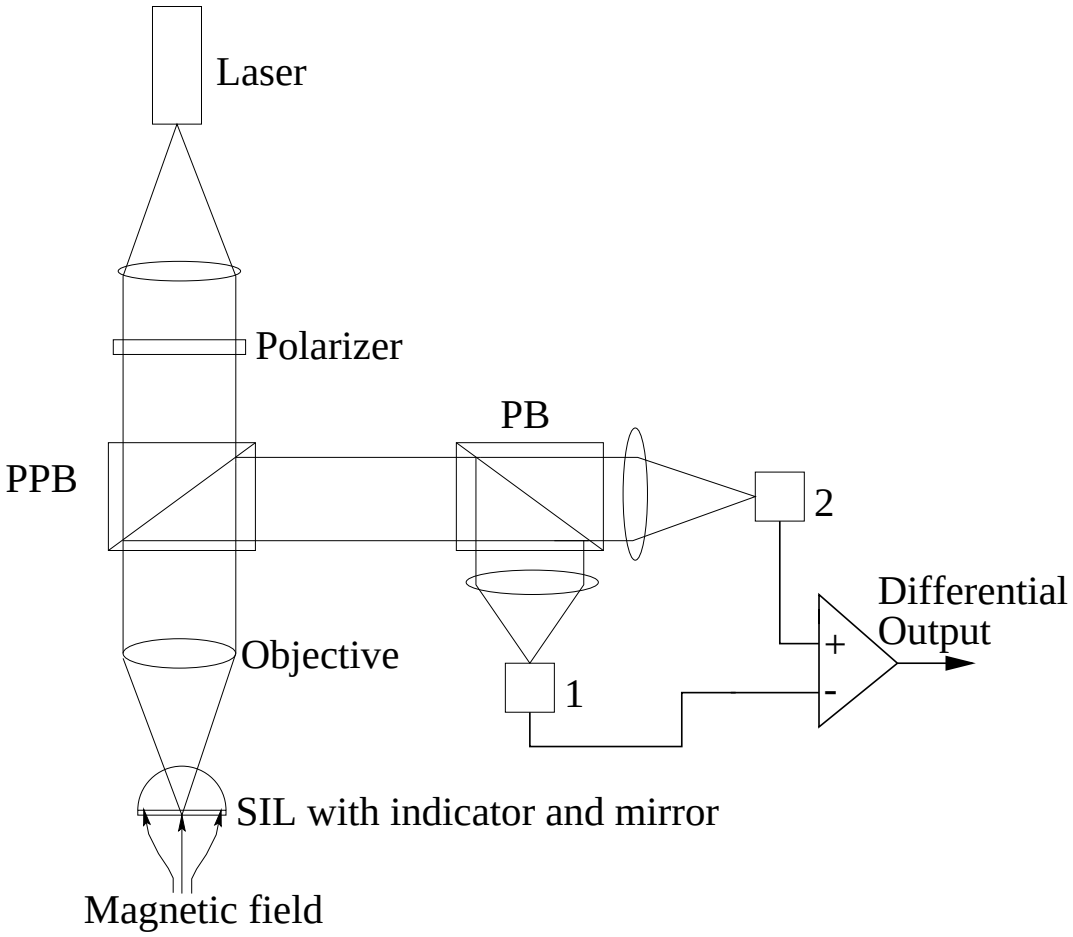
Laser
Polarizer
PB
PPB
2
Differential
Output
+
-
Objective
1
SIL with indicator and mirror
Magnetic field

Figure 2

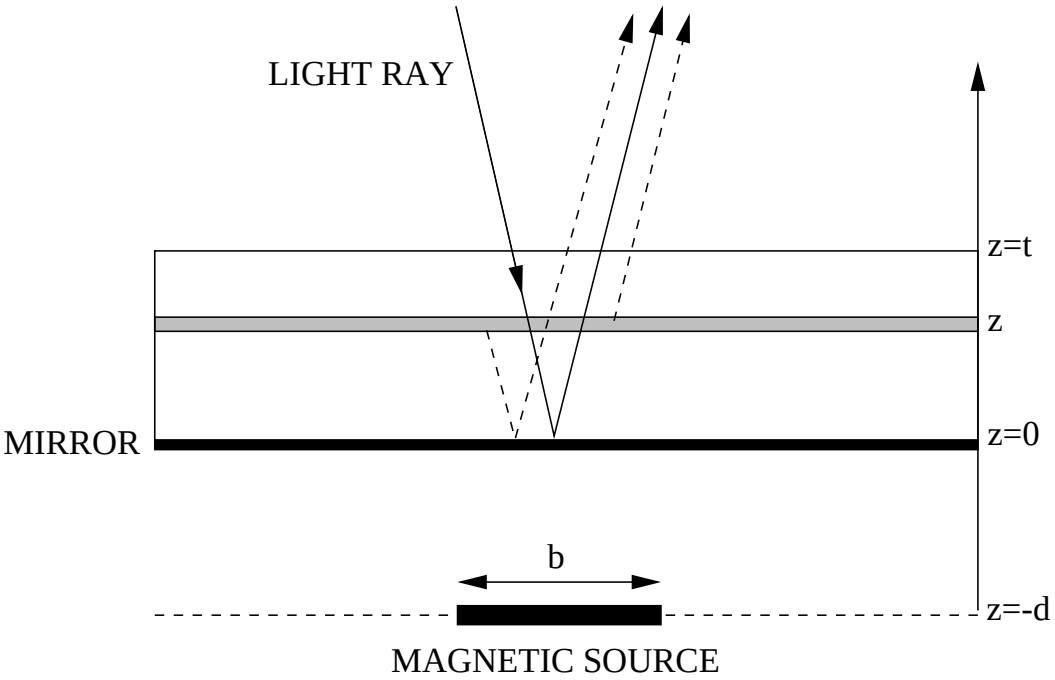

Figure 3

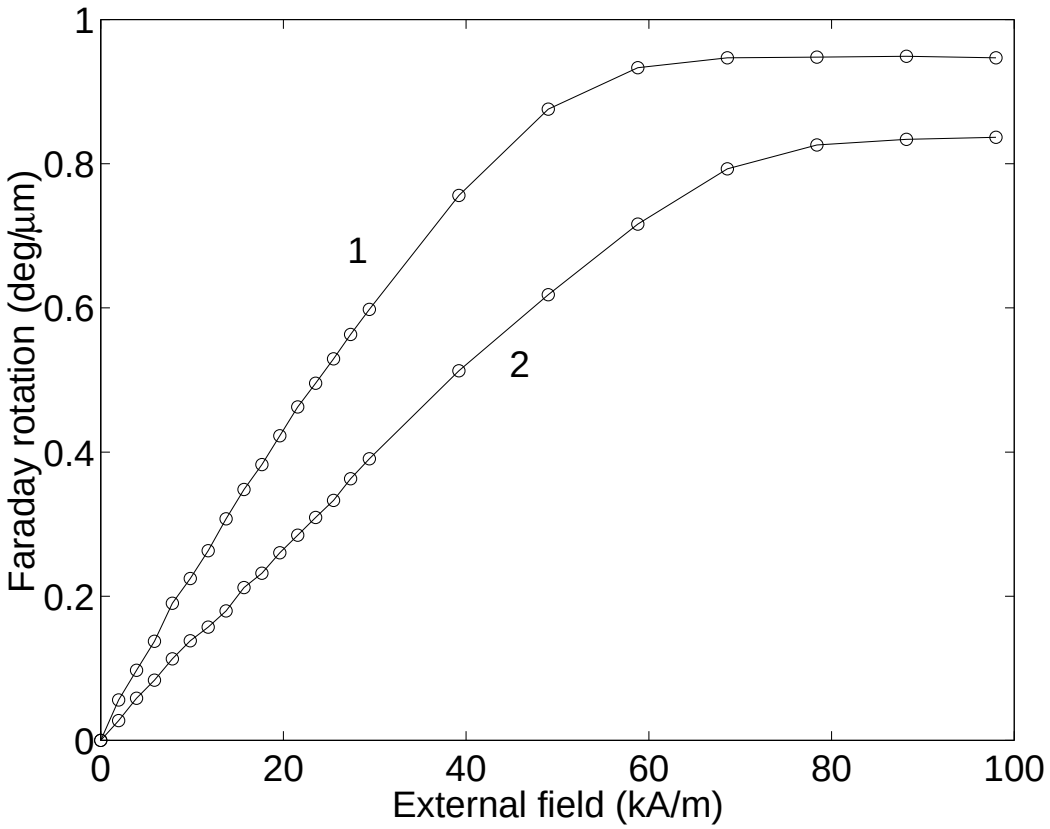
Faraday rotation (deg/μm)
External field (kA/m)
0
0.2
0.4
0.6
0.8
1
0
20
40
60
80
100
1
2

Figure 4

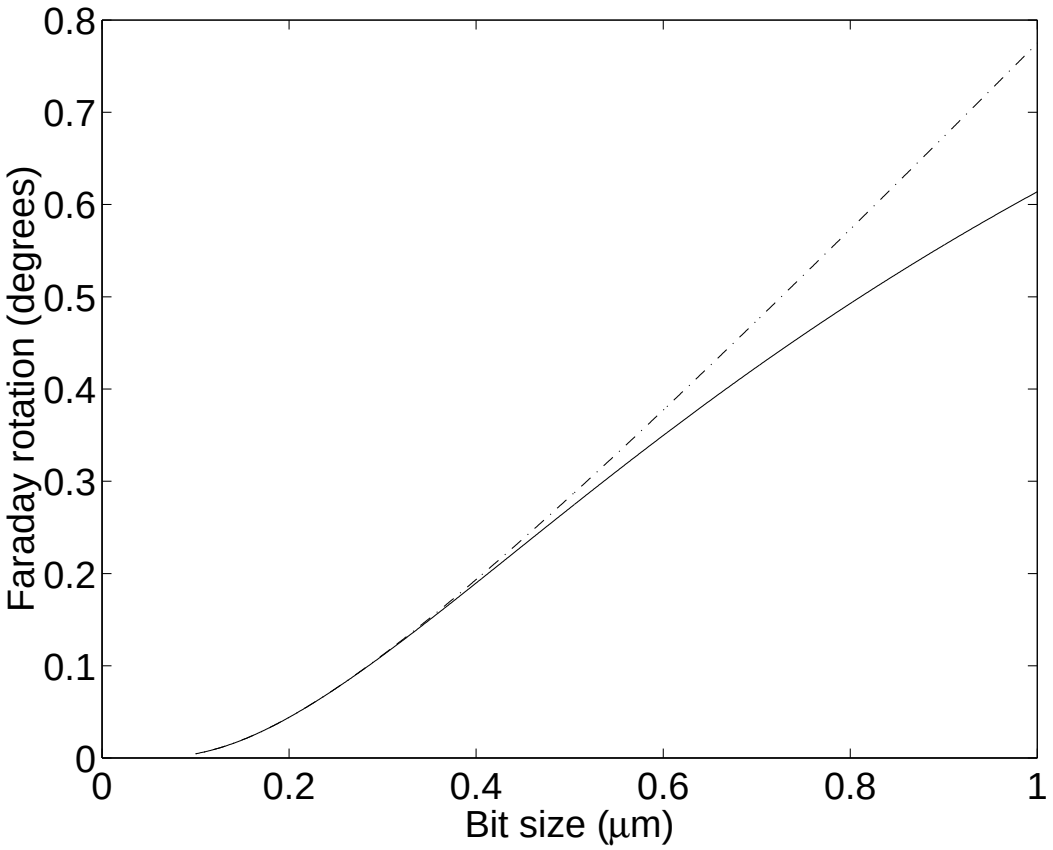
0.8
0.7
0.6
0.5
0.4
0.3
0.2
0.1
0
Faraday rotation (degrees)
0
0.2
0.4
0.6
0.8
1
Bit size (μm)

Figure 5

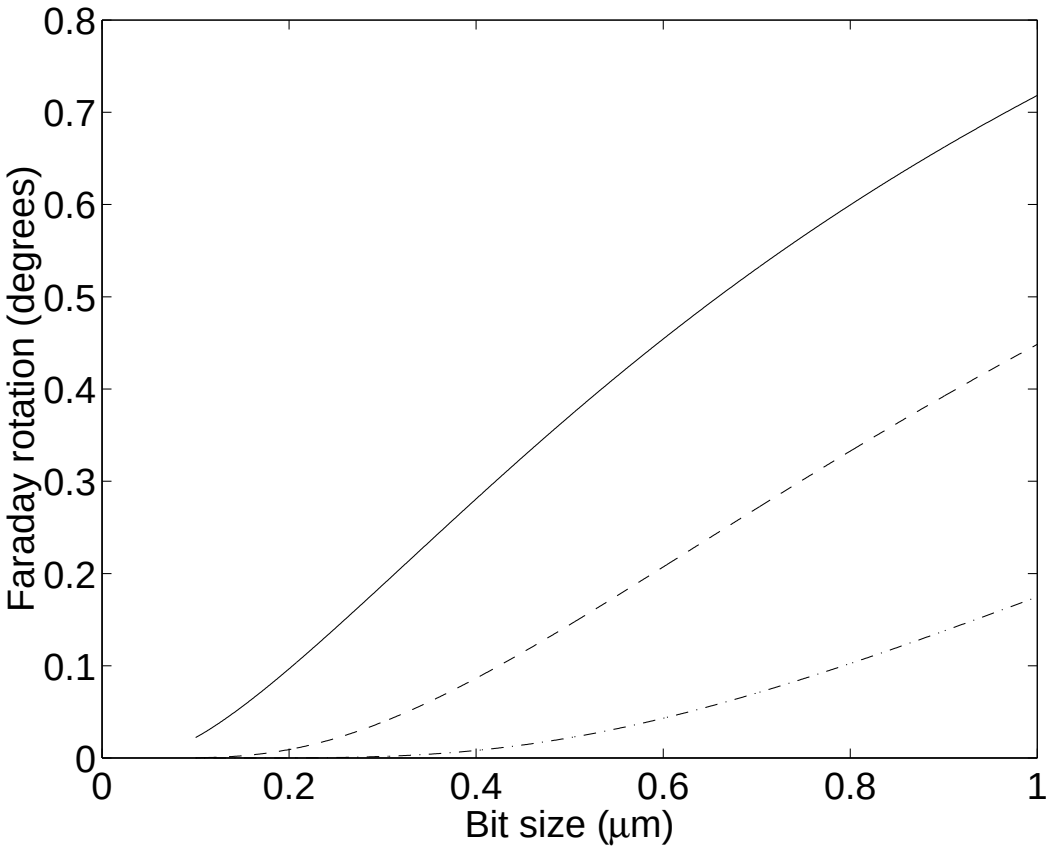
0.8
0.7
0.6
0.5
0.4
0.3
0.2
0.1
0
Faraday rotation (degrees)
0
0.2
0.4
0.6
0.8
1
Bit size (μm)

Figure 6

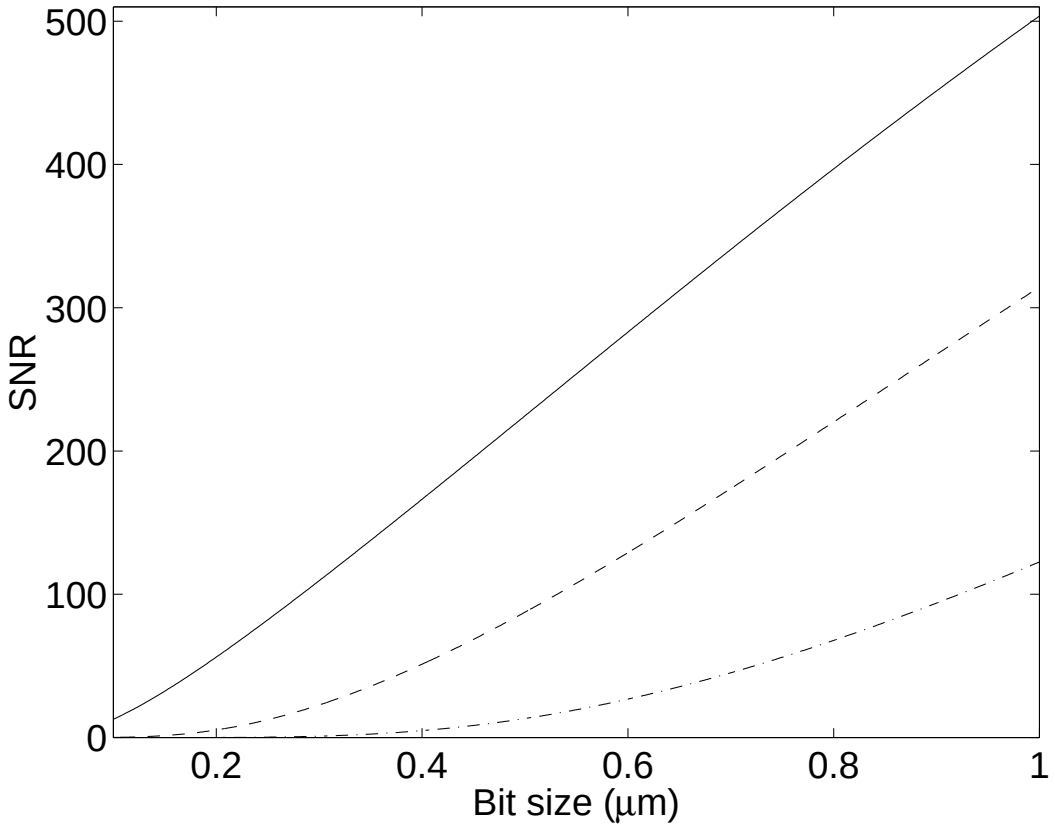

Figure 7

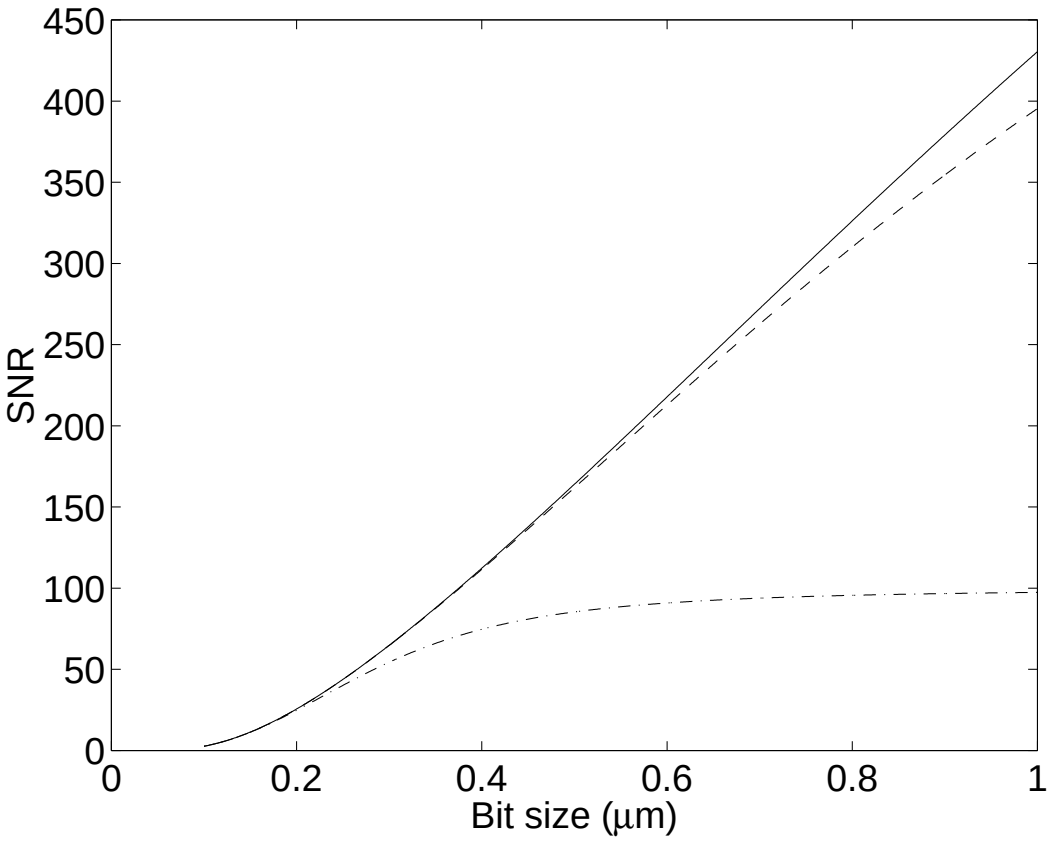

Figure 8

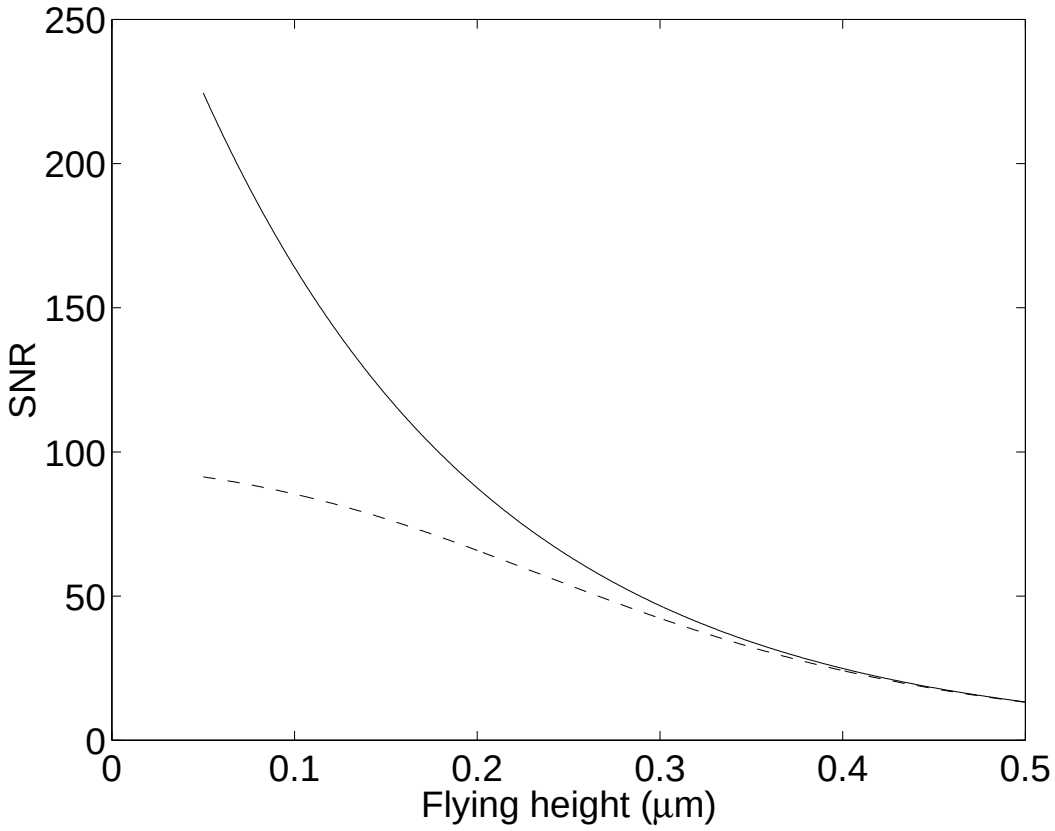

Figure 9

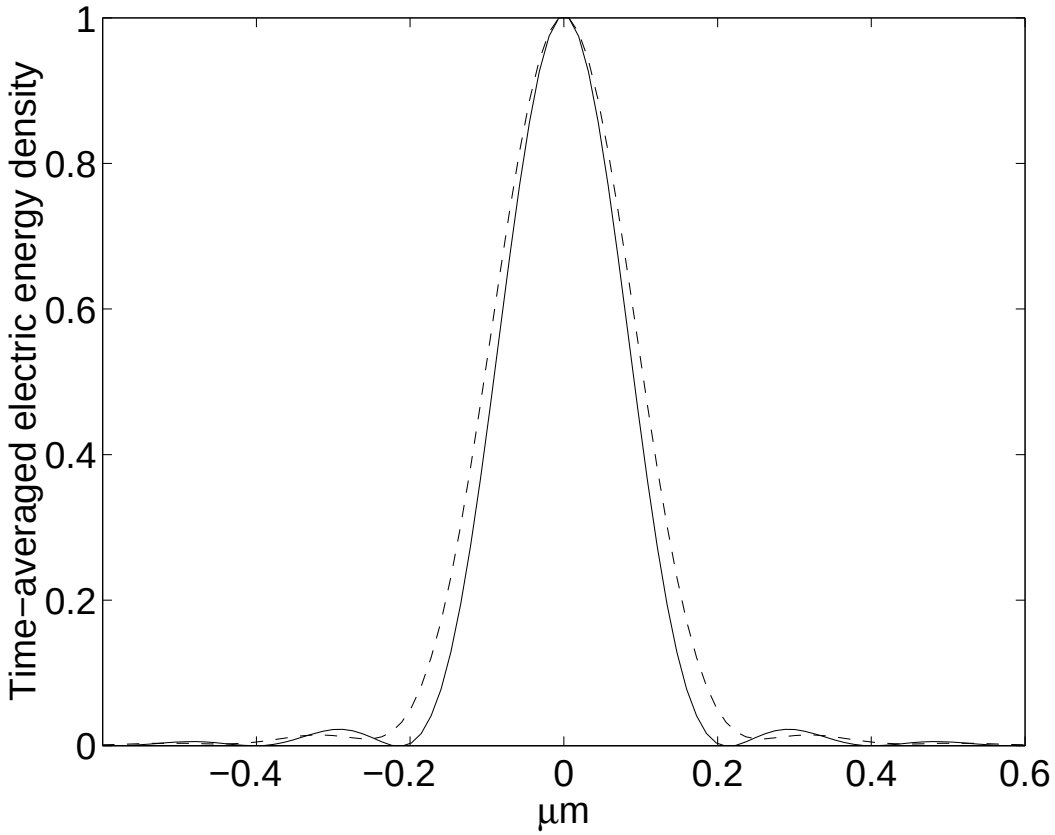
Time−averaged electric energy density
1
0.8
0.6
0.4
0.2
0
−0.4
−0.2
0
0.2
0.4
0.6
μm

Figure 10